CrossMark

Synthesis of Au nanoparticles–decorated CdS nanowires via laser ablation in liquid for optoelectronic applications

Raid A. Ismail[1] · Walid K. Hamoudi[1] · Hadeel F. Abbas[1]

Abstract

Au nanoparticles‒decorated CdS nanowires have been synthesized by laser ablation in liquid under the effect of intense light pulses (IPL). An Nd:YAG laser with 3 J/cm²/pulse energy fluence of 7 ns pulses was combined with (2 J/cm²/pulse) energy fluence of 3 ms intense light pulses and used to ablate Au target in colloidal CdS nanowires. The effect of IPL irradiation on structural, morphological and optical properties of Au NPs–decorated CdS NWs was investigated. Results of optical properties showed an increased optical energy gap from 2.5 to 2.61 eV after combining IPL source with laser ablation pulses. The photoluminescence emission peak of Au NPs‒decorated CdS NWs was blue shifted from 473 to 462 nm with a significant rise in the PL intensity, after using the IPL. The synthesized Au NPs–CdS NW hybrids exhibited high surface-enhanced Raman scattering SERS after being irradiated with IPL. The IPL-assisted laser ablation improved structural characteristics by increasing the photocurrent, reducing structural defects, minimizing the e–h recombination at the junction interface and enhancing the figures of merit of the Au–decorated CdS/Si photodetector.

1 Introduction

Multicomponent nanomaterials have recently received a great attention in many applications such as biosensors, photovoltaic devices, Schottky detectors, lasers, solar cells, memory devices, and light emitters, due to their superior structural, optical, electrical, and magnetic properties [1–3]. The ability to fabricate multicomponent materials in nanoscale size opened new fields in fabricating multifunction materials of novel characteristics which could not be obtained from their bulks [4]. Many forms of these materials have been demonstrated as core–shell and nanocomposites. The enhanced light absorption of semiconducting materials and greater e–h pairs' separation can be obtained by trapping the photo-generated carriers in the metallic part. Core–shell semiconductor–noble metals also allow tailoring surface plasmon resonance (SPR) by electron transfer for visible-enhanced photodetectors [5]. Cadmium sulfide nanowires have superior optical and electrical properties. They had been used in photodetectors, light-emitting diodes, high-rate photo-catalytic hydrogen production, solar cells, and

optical switches. Cu, Ni, In, Mn, Ag, and Au were utilized to decorate CdS nanowires, to obtain superior photo-activity and long-term stability or to form core–shell structure with improved responsivity in the visible region [6]. Au nanoparticles (NPs) are found to be promising co-catalyst to improve CdS photo-catalytic performance (electrochemical applications) [7]. The reported data revealed that the Au–CdS hybrid gives many advantages over pure CdS nanowires such as effective separation of photo-catalytic electrons and holes, large surface area and higher carrier mobility [8, 9]. In addition to the electrochemical applications, Au–CdS hybrid has been used as highly selective biosensor [10]. Self-assembly and solid sulfuration, and facile solvother-mal and deposition are among many routes to prepare Au nanoparticles–decorated CdS nanowires. Compared to these routes, laser ablation of nanomaterials in liquid is efficient, simple, cost effective, and no catalyst or vacuum is required. In addition, it can achieve very pure nanosized materials and good control on size and morphology of the synthesized materials [11]. Laser fluence, wavelength, liquid type and laser pulse duration can affect the size and morphology of the synthesized CdS nanoparticles and nanowires [12]. Up to best of our knowledge, no research work has been reported on decorating CdS nanowires with Au nanoparticles using laser ablation in liquid. Herein, we report such work with improved characteristics by combing the synthesis

✉ Raid A. Ismail
  raidismail@yahoo.com

[1] Department of Applied Science, University of Technology, Baghdad, Iraq

process with intense light pulses. The figures of merit of Au NPs–decorated CdS NWs/Si photodetectors were investigated with and without using IPL. Here, we have used IPL during laser ablation process to control the morphology and Au NP size which are considered very key parameters for designing high-performance Au NPs–decorated CdS NWs/Si photodetector.

2 Experiment

In previous publication, the route details adopted to synthesize colloidal cadmium sulfide nanowires by 1064-nm pulsed Nd:YAG laser ablation of Cd target in thiourea solution were presented [13]. The ablation solution was prepared by mixing together 10 mM thiourea (CH_4N_2S); as a sulfur source, with 50% ethanol; to prevent CdO formation, and (3.57 mM) cetyltri-methyl-ammonium bromide CTAB [($C_{16}H_{33}$)N(CH_3)$_3$]Br as a surfactant. To synthesize Au NPs–decorated CdS NWs, first a gold pellet was ablated in colloidal CdS nanowires using 140 laser pulses from fundamental wavelength Nd:YAG laser, each with 3 J/cm^2 laser fluence and 7 ns duration. 2 J/cm² energy fluence pulses of 3-ms duration were provided by Lab-assembled IPL system to assist laser ablation. The IPL emission was synchronized with the Q-switched Nd:YAG laser pulses by triggering the laser with an optically attenuated IPL pulse. Figure 1a illustrates a schematic of forming Au NPs–decorated CdS NWs

by laser ablation in liquid. The work necessitated the use of CdS colloidal; synthesized by (3 J/cm²) laser energy fluence and combined with (2 J/cm²/pulse) energy fluence from the IPL system. The optical absorption of the Au–decorated CdS NW colloidal solution was measured using UV–Vis double beam spectrophotometer (Shimadzu, 00912901-S.Korea). The structural properties were investigated using X-ray diffractometer (XRD-6000, Shimadzu). Scanning electron microscope SEM (FE-SEM; MIRA3 TESCAN, Razi Metallurgical Research Center, Iran) equipped with energy-dispersive X-ray EDX was also employed to study structural and chemical composition. Raman spectroscopic analysis was conducted using Bruker Raman microscope. Fourier transform infrared spectroscopy FT-IR measurement was carried out using Shimadzu 8000 spectrometer. The shape and size of the CdS and CdS–Au nanocrystals were researched using transmission electron microscope TEM (CM10 pw6020, Philips, Germany). Hall measurement was used to investigate the electrical resistivity and carrier mobility of Au NPs–decorated CdS NW layer. To fabricate Au NPs–decorated CdS NWs/Si photodetector with 5Ωcm electrical resistivity—polished (111) silicon substrate was used. Thin layer of Au NPs–decorated CdS NW hybrids was deposited on silicon substrate by drop casting technique by employing a special mask. After deposition, the substrate was heated at 70 °C under argon. Ohmic contacts were established on the Au NPs–decorated CdS NW layer and silicon by depositing indium and aluminum films using thermal resistive system.
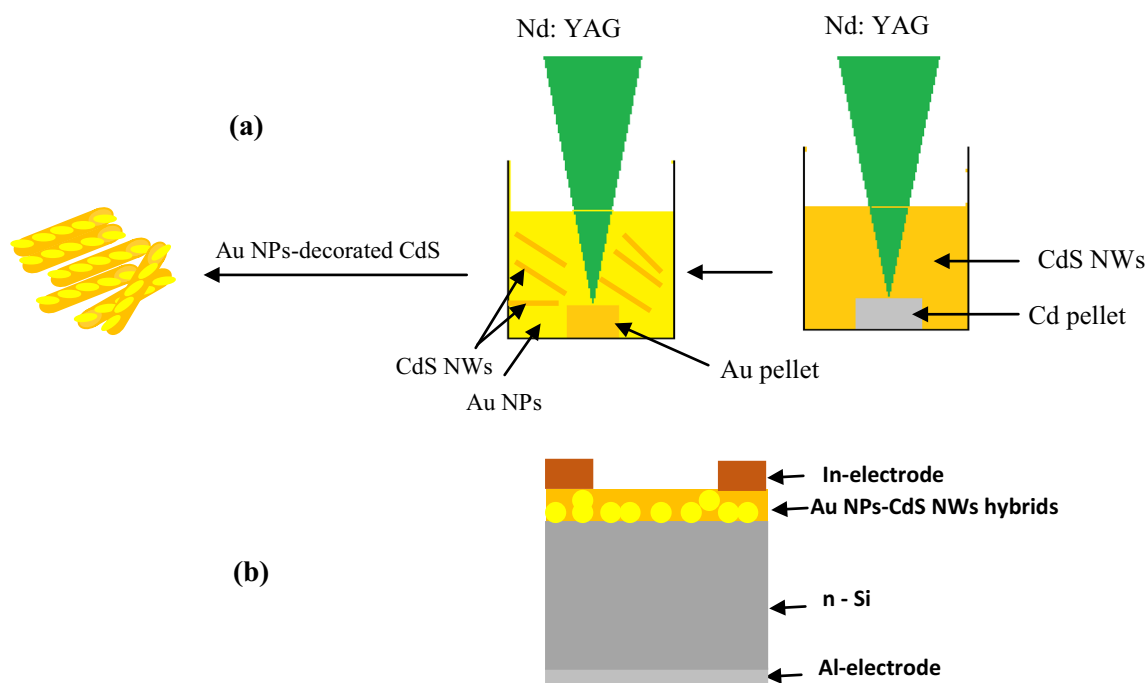

Fig. 1 **a** Schematic diagram of **a** mechanism formation of Au NPs–CdS NW hybrids by two-step laser ablation in liquid and **b** cross-sectional view of Au NPs–decorated CdS NWs/Si photodetector

Figure (1b) displays the architecture of Au NPs–decorated CdS NWs/Si photodetector.

3 Results and discussion

Figure 2 illustrates a freshly prepared colloidal CdS NWs and colloidal Au NPs–decorated CdS NWs synthesized by laser alone and by laser with IPL source. The CdS NWs have bright yellow color which changed into yellowish brown after being decorated with Au NPs; due to the formation of nanocomposite structure.
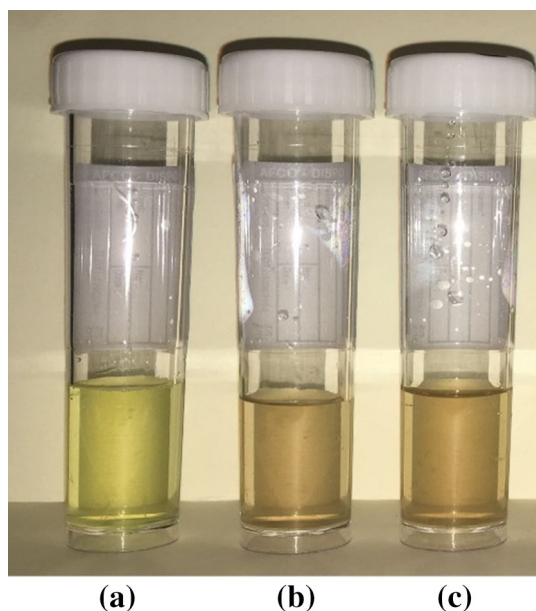

Fig. 2 a Colloidal CdS NWs, **b** Au NPs–decorated CdS NWs synthesized by laser ablation and **c** Au NPs–decorated CdS NWs synthesized by laser ablation and IPL source
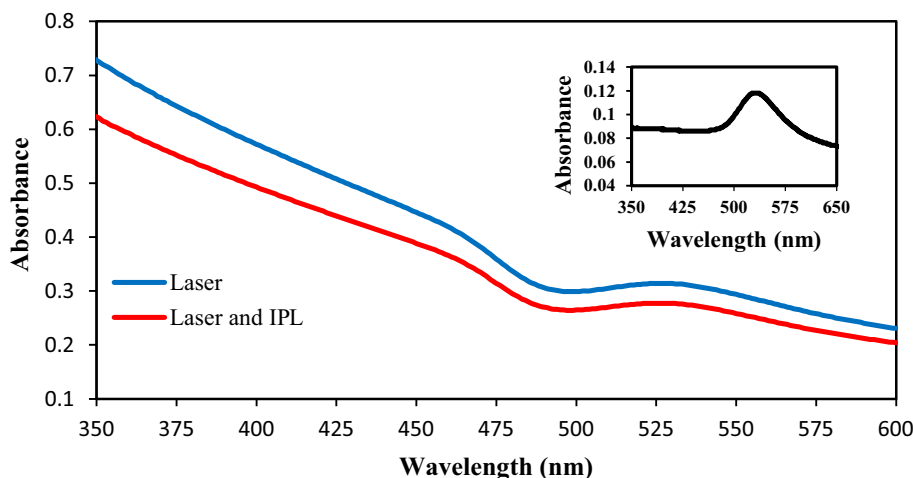
Figure 3 displays the absorption spectra of colloidal Au NPs–decorated CdS NWs prepared with and without IPL source. As shown in the inset, the Au nanoparticles reveal surface plasmon resonance SPR absorption peak around 546 nm. Due to SPR, the Au NPs were heated and melted by the high-intensity laser pulses [14]. This facilitated the deposition of Au NPs on CdS NWS and the production of Au NPs–decorated CdS NW structure. The optical absorption of Au NPs–CdS NW hybrids exhibited broadened SPR peak with a small blue shift indicating heterostructure formation. This is ascribed to the high dielectric coefficient and exciton–plasmon coupling of nanostructured CdS which changed the SPR peak of the Au NPs [15–17]. Figure 3 also confirms a decreased optical absorption because of the decreased particle size after combining IPL with laser pulses. No significant shift in the SPR of Au NPs–CdS NW hybrids was observed with this IPL–laser combination. The optical absorption of Au NPs–CdS NW hybrids synthesized with and without IPL decreased with the wavelength in the same manner. The optical energy band gap of the Au NPs–CdS NW hybrids was estimated by extrapolating the linear part of $(\alpha h\nu)^2$ versus photon energy plot to $(\alpha h\nu)^2 = 0$ points as shown in Fig. 4.

It is found that the optical energy gap increased from 2.5 to 2.62 eV (blue shift) because of the decreased particle size after combining the IPL pulses with the laser. In Fig. 5, the PL emission spectra of Au NPs–decorated CdS NWs show a weak broad PL emission peak centered at 473 nm corresponding to 2.62 eV which originates from e–h recombination. The intensity of this broad peak is much stronger than that of Au NPs–decorated CdS NWs synthesized without using IPL. This can be ascribed to the decreased agglomeration of Au NPs and CdS NWs. In addition, 10-nm blue shift was seen after using IPL due to the decreased dimensions of the Au NPs and CdS NWs. The PL results are in good agreement with the results of UV–Vis.
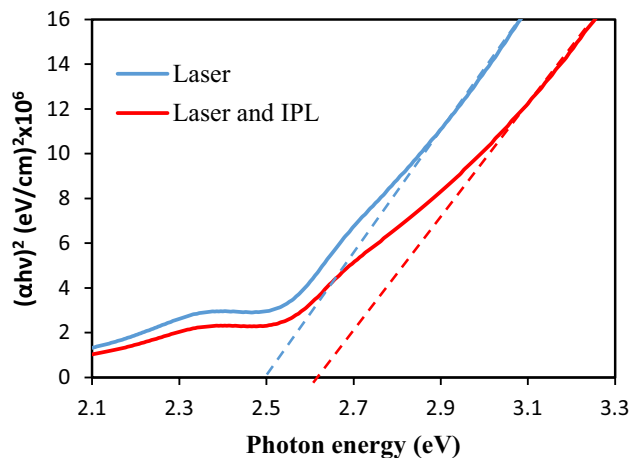
Fig. 3 Absorption spectra of Au NPs–CdS NW hybrids. Inset is the optical absorption of Au NPs

Fig. 4 Plot of $(\alpha h\upsilon)^2$ vs. $h\upsilon$ of Au-CdS hybrids with and without IPL
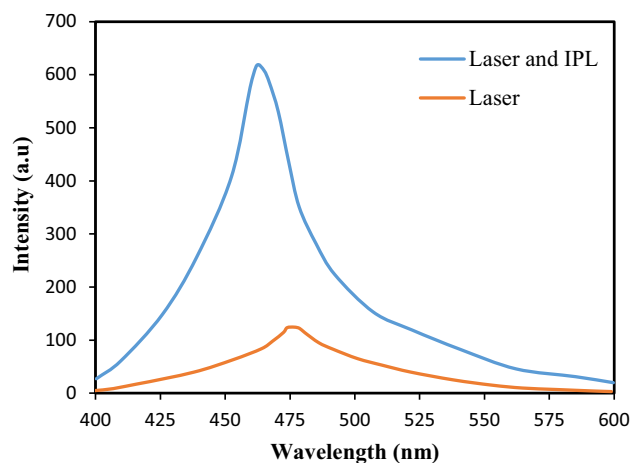
Fig. 5 Room temperature PL emission spectra of Au NPs-CdS NWs

Fig. 6 XRD patterns of Au NPs–decorated CdS NWs
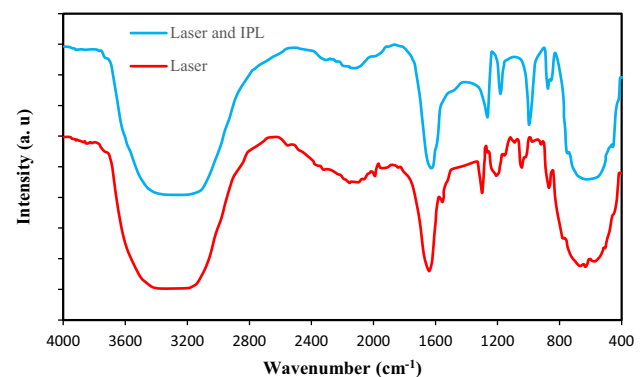
Fig. 7 FT-IR spectra of Au NPs–CdS NW hybrids

Figure 6 illustrates the XRD patterns of Au NPs–CdS NW hybrids with and without using IPL. Five reflection peaks were observed. The peaks at 38.2° and 44.5°, corresponding to (111) and (200) reflection planes, are related to cubic Au NPs with face-centered cubic structure according to JCPDS # 00-04-0784. This result indicates well crystallization of Au NPs and good adhering on the CdS NWs which confirm the formation of Au NPs–CdS NW hybrid structure [18].

The reflection peaks at 26.5°, 28.7° and 43.75°; corresponding to (101), (102) and (110) belong to the hexagonal CdS NWs according to JCPDS # 00-041-1049. New peak at 24.8°, corresponding to (002) reflection plan, is related to hexagonal CdS appearing after combining IPL with laser, which indicates a growth of CdS NWs perpendicular to the c-axis. It suggests that the IPL pulses helped the formation of highly oriented and better crystallinity CdS NWs along
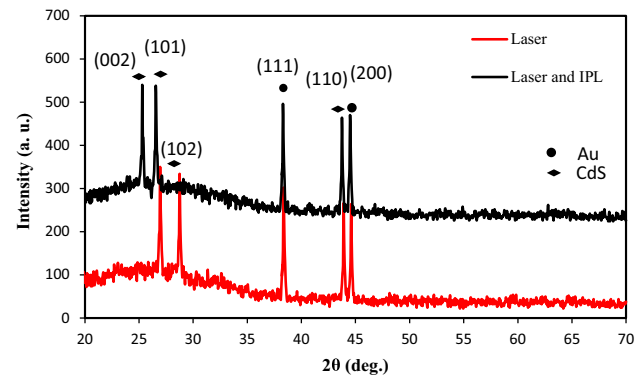
the c-axis direction by providing an external electromagnetic field to the synthesized CdS NWs. Small shift in the (101) reflection plane was observed after combining IPL with laser due to small off-stoichiometry CdS NWs. No reflection peaks related to AuCd or Au_2S phases were noticed in the XRD patterns with or without IPL; indicating the formation of only Au NPs–decorated CdS NW structure [18]. The FT-IR transmission spectra of the Au NPs–decorated CdS NWs in the (400–4000) cm^{-1} range are depicted in Fig. 7. All spectra illustrate almost the same chemical bonds; hence, they show very strong absorption broad band at (3150–3500) cm^{-1} belonging to O–H stretching vibration of water molecules. In addition, there is a strong absorption peak at 1635 cm^{-1}; indexed to the bending vibration of water molecules [19].

There is also a strong absorption band at (525–700) cm^{-1} can be assigned to CdS stretching vibration [20]. The weak broad peak at (2000–2400) cm^{-1} indicates the presence of C≡C stretching band. No significant intensity variation of the full width absorption peaks at half maximum was noticed after combining the IPL source. The strong peak at 980 cm^{-1} and the weak peak at 722 cm^{-1} are ascribed to the presence of bending vibration of CdS [21]. C–O stretching
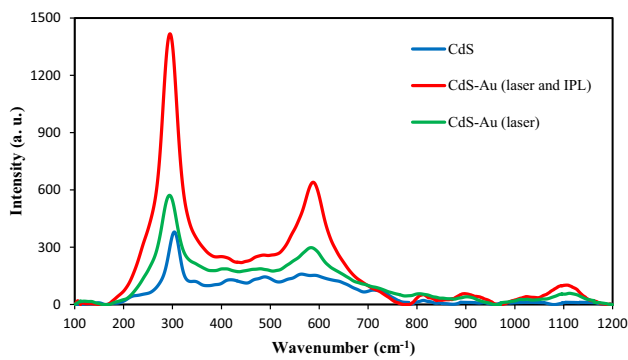
Fig. 8 Raman spectra of CdS NWs and Au NPs–decorated CdS NWs

vibration was identified at 1200 cm^{-1} and the strong peak at 1264 cm^{-1} can be indexed to the C(O)–O stretching vibrations. The FT-IR spectrum of Au NPs–CdS NW hybrids suggests strong-intensity absorption bands with small shift towards the small wavenumber. Raman Au NPs–CdS NW hybrid spectra in Fig. 8 reveal two main peaks at 300 cm^{-1} and 600 cm^{-1} corresponding to first-order (1LO) and second-order (2LO) CdS longitudinal optical phonon modes, respectively. These two modes couple to excitons along the CdS crystal axis. Other Raman modes are attributed to multi-phonon responses relating transverse and longitudinal acoustic phonons [22].

Without Au decoration, weak fundamental and harmonic Raman peaks originate from CdS NWs. The Raman intensity has increased after Au NP decoration due to surface-enhanced Raman scattering (SERS). Increasing the SERS activity, after Au NP decoration, is attributed to the existence of large densities of nanowires and nanoparticles which helped supplying large numbers of localized surface plasmons (LSPs) [23]. Figure 8 also confirms Raman intensity enhancement after combining IPL with laser ablation due to the enhancement of local electric field near the non-aggregated Au NPs [24]. The EDX spectra of Au–decorated CdS NW structures synthesized by laser alone and by combining IPL source with the laser are given in Fig. 9. The EDX analysis confirmed the existence of Cd, S, and Au elements in addition to O and Si, originated from the glass substrate. This result confirms the creation of Au NPs–CdS NW hybrids. The Au weight percentage increased and the [Cd]/[S] ratio changed slightly after using IPL.

TEM imaging was employed to get detailed insight of the morphology and microstructure of the Au NPs–CdS. Figure 10 shows a TEM image of Au NPs–CdS NW hybrids, in which some 15-nm-average-sized Au NPs are adhered on the surface of CdS NWs. The TEM image confirms the formation of few-micron-long mono-dispersed CdS NWs with an average diameter of 35 nm. This figure also shows some aggregated gold nanoparticles dispersed on the CdS NWs. Production of Au nanoparticles with different sizes arises
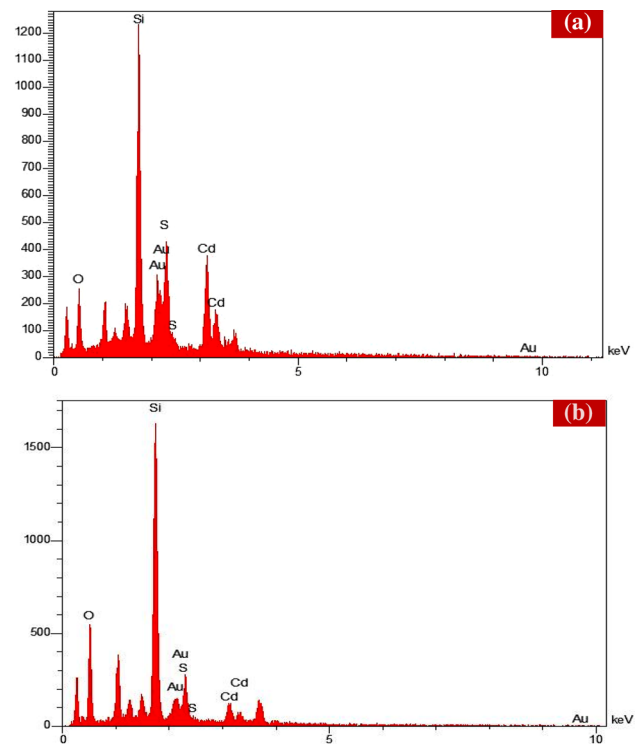

Fig. 9 EDS spectra of Au–CdS core–shell synthesized by **a** laser and **b** laser and IPL

from the Gaussian distribution of laser beam [25]. Aggregation and agglomeration of Au NPs were decreased after combining the IPL with laser as shown in Fig. 10b. In fact uniform distribution of Au NPs on the surface of the CdS NWs is seen. The IPL pulses helped increasing the surface coverage area of Au NPs on the CdS NWs, and also helped improving the electrostatic attraction between Au NPs and CdS NWs. Figure 11 illustrates the effect of IPL on dark current–voltage (I–V) characteristics of Au NPs–CdS NWs/Si heterojunction at room temperature.

The forward current increases exponentially with bias voltage, and the reverse current did not depend on voltage. The use of IPL has reduced the electrical resistivity of the Au NPs–decorated CdS NW layer arises from increasing the CdS nanowire length, which in turn, increased the forward current. Hall measurement revealed that the electrical resistivity of Au NPs–decorated CdS NW layer decreased from 6.81×10^3 to 2.5×10^3 Ω cm and the carrier mobility increased from 173 to 375 cm^{2}V^{-1}s^{-1} after using IPL. In addition, the rectification characteristics of the heterojunction were enhanced and, therefore, the rectification factor increased from 35 to 56 at 5 V. To evaluate the junction characteristics, the ideality factor was calculated from forward characteristics and found to be 3.3 and 2.7 with and without using IPL. The value of ideality factor of Au NPs–CdS NWs/Si heterojunctions with and without IPL was smaller

Fig. 10 TEM micrographs of **a** Au NPs–decorated CdS NWs synthesized by **a** laser only, and laser and IPL (**b**)
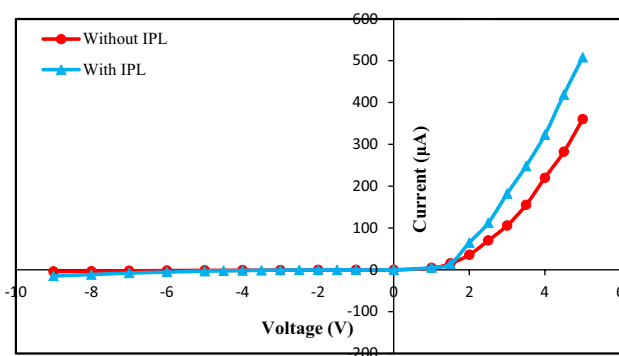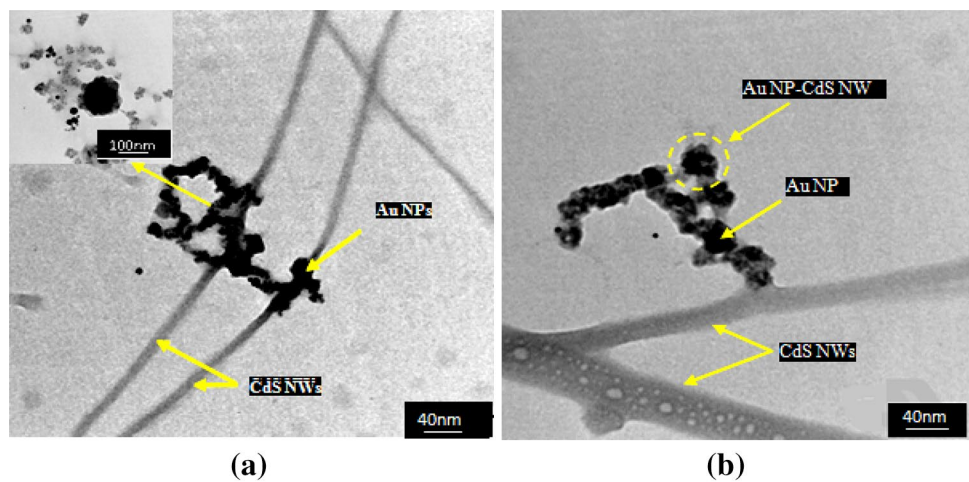

(a)

(b)

Fig. 11 Dark I–V characteristics of Au NPs–CdS NWs/Si heterojunction photodetector

Fig. 12 Illumination I–V characteristics of Au NPs–CdS NWs/Si photodetector

than that of CdS/Si heterojunctions prepared by laser ablation in liquid and by chemical bath deposition [13, 26] due to decreasing the surface state defects and trapping centers thorough the presence of Au nanoparticles which act as carrier traps.

This improvement in junction characteristics can be attributed to the reduction in the structural defects and the recombination process at the junction interface. The illuminated I–V characteristics of heterojunction photodetectors is given in Fig. 12. The on/off ratios of Au NPs–CdS NWs/Si heterojunctions prepared with and without IPL were 468 and 343 at 5V, respectively. These values are larger than those of CdS NWs/Si heterojunctions prepared by successive ionic layer adsorption [27]. Figure 12 confirms that the photocurrent was increased by factor of 1.47 at 5V after combining IPL with the laser. Increasing the photocurrent arises from absorption of the large amount of visible light and the presence of large electric field that prevents e–h pair recombination. Figure 13 shows the responsivity as a function of wavelength of the Au NPs–CdS NW/Si heterojunction photodetector with and without using IPL. For Au NPs–decorated CdS NWs/
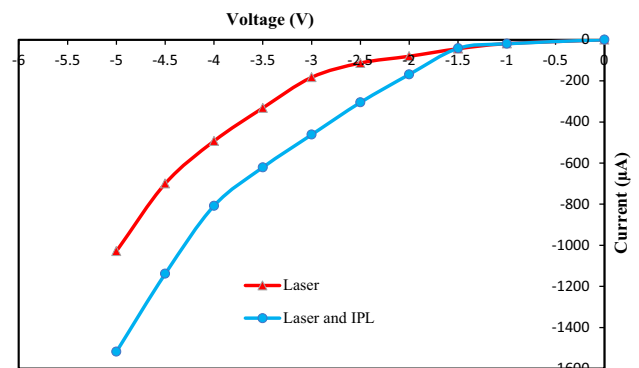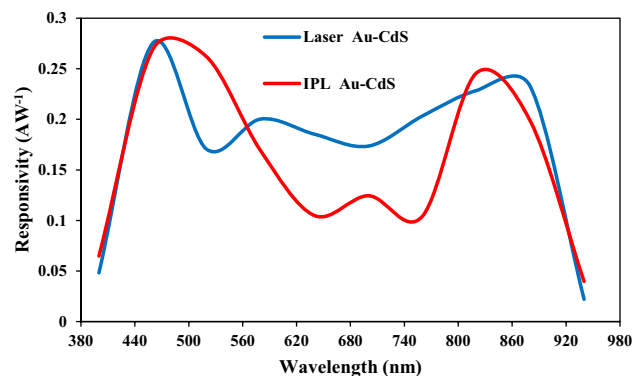

Fig. 13 Effect of IPL on the responsivity of Au NPs–CdS NWs/Si hybrid photodetector

Si photodetector synthesized without IPL, three response peaks were found at 460 nm, 580 nm, and 880 nm with responsivity of 0.27 A/W, 0.2 A/W, and 0.23 A/W, respectively. The first and second peaks are due to the absorption
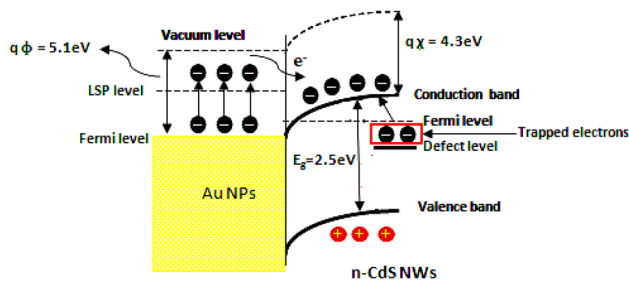
Fig. 14 Energy band diagram of Au NPs–CdS NW hybrids

edge of CdS and Au–CdS hybrids and the third peak belongs to the absorption edge of the silicon substrate.

The responsivity at the visible region is higher than that of CdS/Si heterojunction due to electron transfer from localized surface plasmon LSP level in Au NPs to the conduction band of Cd NWs (see Fig. 14). As a result, more free electrons have transferred which increased the photocurrent [28]. The decoration of Au NPs on the CdS acts as carrier traps to reduce the e–h recombination process [29]. Electrons trapped by donor-like level (defect level) have also been transferred to conduction band of CdS NWs and further enhanced the photocurrent. After using IPL, the response peaks were noticed at 460 nm, 700 nm, and 820 nm with spectral responsivity of 0.27 A/W, 0.12 A/W, and 0.24 A/W, respectively. The reported data showed that the CdS/Si NW heterojunction photodetector grown by pulsed laser deposition technique has three peaks of response at 469 nm, 700 nm and 953 nm [30]. Figure 13 indicates that the IPL helped the photodetector to respond better for the 410–630-nm region.

4 Conclusion

We have successfully synthesized crystalline Au NPs–CdS NW hybrids by two-step laser ablation in liquid. The effect of IPL on optical and structural properties of Au NPs–decorated CdS NWs was demonstrated. XRD data revealed crystalline hexagonal Au NPs–decorated CdS NWs. Combining IPL with laser ablation allowed a significant enhancement in Raman peak intensity after decorating the CdS NWs with Au NPs due to surface-enhanced Raman scattering (SERS). Strong fundamental Raman peaks, suited at $300\ cm^{-1}$ (1LO), and weak overtone one, located at around $600\ cm^{-1}$ (2LO), were seen. EDX analysis confirmed the existence of Cd, S, and Au elements. The TEM observation confirmed the formation of Au–decorated CdS NW structure with 15-nm-average-sized Au NPs and 35 nm average diameter of CdS NWs. The decoration (distribution and adherence) of Au NPs on the CdS NWs has enhanced the photodetector photosensitivity when using

IPL through the reduction of the recombination rate and the increase of the carrier collection efficiency. The on/off ratios of Au NPs–CdS NWs/Si heterojunction prepared with and without IPL were 468 and 343 at 5V, respectively. Using IPL, the figures of merit of Au NPs–CdS NWs/Si photodetector were improved with good wavelength response selectivity. The Au NPs–CdS NWs/Si hybrid photodetector exhibited three peaks of response located at 460 nm, 700 nm, and 820 nm. To best of our knowledge, this is the first study in which IPL source is combined with the laser to manufacture CdS NW photodetectors with better characteristics. The additional advantages can push the performance of the CdS photodetectors higher in terms of photosensitivity and figures of merit.

References

1. V. Chumachenko, A. Naumenko, O. Yeshchenko, N. Kutsevol, I. Bondarchuk, J. Nanomater. **2016**, 1 (2016)
2. W. Chen, T. Yang, Y. Hsu, Chem. Mater. **20**, 7204 (2008)
3. K. Easawi, M. Nabil, T. Abdallah, S. Negm, H. Talaat, Int. J. Mater. Metall. Eng. **6**, 63 (2012)
4. E. Khon, A. Mereshchenko, A. Arnovsky, K. Acharya, A. Klinkova, N. Kasakarage, I. Nemitz, M. Zamkov, Nano Lett. **11**, 1792 (2011)
5. G. Bajaj, R. Soni, Appl. Surf. Sci. **256**, 6399 (2010)
6. R. Singh, B. Pal, Part. Sci. Technol. Int. J. **33**, 53 (2015)
7. Z. Yu, Y. Xie, G. Liu, G. Lu, X. Ma, H. Cheng, J. Mater. Chem. A **1**, 2773 (2013)
8. S. Han, L. Hu, N. Gao, A. Ghamdi, X. Fang, Adv. Funct. Mater. **24**, 3725 (2014)
9. S. Liu, Y. Xu, Nanoscale **5**, 9330 (2013)
10. W. Zhang, J. Zheng, C. Tan, X. Lin, S. Hu, J. Chen, X. You. S. Li, J. Mater. Chem. B **3**, 217 (2015)
11. J. Seely, B. Kjornrattanawanich, E. Holland, R. Korde, Opt. Lett. **30**, 3120 (2005)
12. R. Ismail, K. Khashan, R. Mahdi, Mater. Sci. Semicond. Process. **68**, 252 (2017)
13. R. Ismail, W. Hamoudi, H. Abbas, Mater. Res. Express **5**, 25017 (2018)
14. X. Phuoc, M. Chyu, J. Mater. Sci. Nanotechnol. **1**, 1 (2013)
15. G. Manna, R. Bose, N. Pradhan, Angew. Chem. Int. Ed. **53**, 1 (2014)
16. D. Mongin, E. Shaviv, P. Maioli, A. Crut, U. Banin, N. Fatti, F. Vallee, ACS Nano **6**, 7034 (2012)
17. X. Wang, Y. Ying, P. Hu, J. Lei, X. Peng, Appl. Phys. A **120**, 1291 (2015)
18. L. Xiao-Li, L. Shan, L. Min, Y. Xue, Z. Li, W. Quan, Chin. Phys. Lett. **31**, 064203 (2014)
19. R. Ismail, B. Rasheed, E. Salm, M. Al-Hadethy, J. Mater. Sci. Mater. Electron. **18**, 397 (2007)
20. N. Ramamurthy, R. Kumar, G. Murugadoss, Nanosci. Nanotechnol. Int. J. **3**, 12 (2011)
21. E. Esakkiraj, S. Abdul Kadhar, J. Henry, K. Mohanraj, S. Kannan, S. Barathan, G. Sivakumar, Optik **124**, 5229 (2013)
22. R. Venugopal, P. Lin, C. Liu, Y. Chen, J. Am. Chem. Soc. **127**, 11262 (2005)
23. J. Suh, J. Lee, Chem. Phys. Lett. **281**, 384 (1997)

24. A. Pimentel, A. Araújo, J. Coelho, D. Nunes, J. Oliveira, J. Mendes, H. Águas, R. Martins, E. Fortunato, Materials **10**, 1351 (2017)

25. R. Ismail, E. Salim, W. Hamoudi, Mater. Sci. Eng. C **33**, 47 (2013)

26. V. Nevruzoglu, M. Tomakin, E. Keskenler, G. Ozturk, J. Ceram. Process. Res. **18**, 494 (2017)

27. Y. Jiang, C. Li, W. Cao, Y. Jiang, S. Shang, C. Xia, Phys. Chem. Chem. Phys. **17**, 16784 (2015)

28. J. Hwang, M. Lai, H. Chen, M. Kao, IEEE Photonics Technol. Lett. **15**, 1023 (2014)

29. I. Zarazúaa, D. Esparzaa, T. López-Lukea, A. Ceja-Fdeza, J. Reyes-Gomezb, I. Mora-Seróc, E. de la Rosaa, Electrochim. Acta **188**, 710 (2016)

30. S. Manna, S. Das, S. Mondal, R. Singha, S. Ray, J. Phys. Chem. C **116**, 7126 (2012)